

Analysis of a Frequency-Hopping Millimeter-Wave Cellular Uplink

Don Torrieri, *Senior Member, IEEE*, Salvatore Talarico, *Member, IEEE*,
and Matthew C. Valenti, *Senior Member, IEEE*.

Abstract

Fifth-generation (5G) cellular networks are expected to exhibit at least three primary physical-layer differences relative to fourth-generation ones: millimeter-wave propagation, massive antenna arrays, and densification of base stations. As in fourth-generation systems, such as LTE, 5G systems are likely to continue to use single-carrier frequency-division multiple-access (SC-FDMA) on the uplink due to its advantageous peak-to-average power ratio. Moreover, 5G systems are likely to use frequency hopping on the uplink to help randomize interference and provide diversity against frequency-selective fading. In this paper, the implications of these and other physical-layer features on uplink performance are assessed using a novel millimeter-wave propagation model featuring distance-dependent parameters that characterize the path-loss, shadowing, and fading. The analysis proceeds by first fixing the location of the mobile devices and finding the performance conditioned on the topology. The spatially averaged performance is then found by averaging with respect to the location of the mobile devices. The analysis allows for the use of actual base-station topologies and the propagation model can leverage empirical millimeter-wave measurements. The benefits of base-station densification, highly directional sectorization, frequency hopping, a large available bandwidth, and a high code rate are illustrated. The minor importance of fractional power control is shown.

Portions of this paper were presented at the 2015 IEEE Military Communications Conference [7]. D. Torrieri is an electrical engineer and mathematician (email: dtorrieri@verizon.net). S. Talarico was with West Virginia University, Morgantown, WV, U.S.A, and he is now with Huawei Technologies, Santa Clara, CA, U.S.A (email: salvatore.talarico81@gmail.com). M. C. Valenti is with West Virginia University, Morgantown, WV, U.S.A (email: valenti@ieee.org).

Index Terms

Millimeter-wave cellular networks, frequency hopping, antenna directivity, stochastic geometry.

I. INTRODUCTION

It is considered likely that 5G cellular networks will operate in millimeter-wave bands [1], [2]. However, the basic structure of the fourth-generation (4G) single-carrier frequency-division multiple-access (SC-FDMA) uplink systems will likely be maintained due to the critical importance of transmitter power efficiency, which is enabled by the low peak-to-average power ratio of SC-FDMA and similar single-channel modulations [3], [4]. It is also likely that 5G systems will exploit frequency hopping to compensate for frequency-selective fading and to randomize out-of-cell interference, as is done in 4G systems [5]. Other likely features of 5G networks include the use of multi-tier heterogeneous networks (HetNets) and the decoupling of the uplink and downlink [6]. On the downlink, biasing is used in a HetNet to expand the range of small cells, thereby balancing cell loads. When the uplink and downlink are coupled, such biasing can cause a mobile device to transmit to a distant base station, which is not optimal from the uplink perspective. However, if the uplink and downlink are decoupled, then the mobile device is free to transmit to a closer base station. Because of blockages and severe shadowing, the base station that receives the strongest signal from a mobile device is not necessarily the one that is closest to it. Thus, in a millimeter-wave network with a decoupled uplink, it is advantageous for the mobile device to establish an uplink with the base station that receives its signal with the greatest strength.

This paper provides a performance analysis of a frequency-hopping millimeter-wave uplink that can serve as the uplink of a fifth-generation (5G) cellular network in its primary mode of operation. The work contained in this paper further elaborates and improves on the analysis of [7]. To drive the analysis, a novel millimeter-wave propagation model is proposed with distance-dependent parameters that characterize the path-loss, shadowing, and fading. The distance dependence of these models accounts for the fact that mobiles close to the BS have a line-of-sight (LOS) path, but the more distant mobiles do not. One of the main goals is to examine the impact of base station (BS) or cell densification, which is the increase in the number of BSs or cells relative to the number of mobiles served. A major benefit of densification is to bring each mobile

closer to its serving BS. Another benefit of densification is that it allows each mobile in a cell access to a larger portion of the available spectrum without causing intrasector interference.

The analysis proceeds by deriving the *conditional* outage probability of the uplink, where the conditioning is with respect to an arbitrary network topology. In the numerical examples, we use an actual BS deployment. Each simulation trial generates a network realization in which the mobile placements are drawn from the uniform clustering distribution [8], while the locations of the BSs remain fixed. For each realization of the network, the outage probability is computed by using closed-form equations for a reference link. By averaging over many mobile station placements, the average outage probability and other statistical performance measures are computed for the given BS deployment. The benefit of this approach relative to other approaches based on stochastic geometry is that it captures the fact that mobiles do not maintain fixed positions, but BSs do. The analysis in this paper applies the methodology and model of [8], which we call *deterministic* geometry to contrast it with stochastic geometry [9], [10]. The two approaches are connected in [11], which proves that deterministic geometry yields the same spatial averages as stochastic geometry. Deterministic geometry can accommodate arbitrary finite topologies with distance-dependent path loss, shadowing, and fading models without making the many typical approximations of stochastic geometry, such as assuming that the fading is the same for all links, or that the topology is drawn from a Poisson point process (PPP) or determinantal point process (DPP) [12]. Moreover, deterministic geometry is able to seamlessly capture the effects of thermal noise, which will be shown to be more detrimental than the interference, and is included in the model without any approximation.

The remainder of the paper is as follows. Section II presents the network model, which includes descriptions of the network topology, the propagation model, sectorization and beamforming, frequency hopping, intrasector and intersector interference, spectral assignments, and power control. Section III presents the equations governing the calculation of the conditional outage probability. Some numerical evaluations for a typical 5G cellular network are given in Section IV. Conclusions are drawn in Section V.

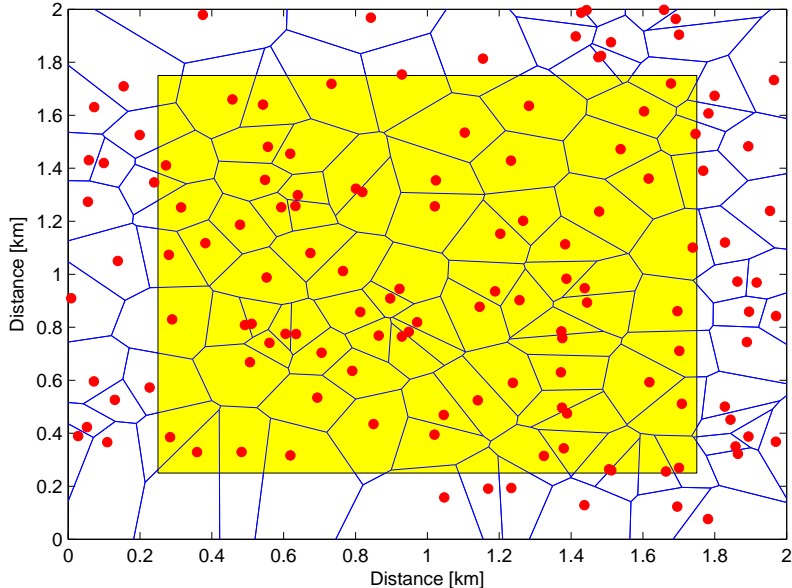


Fig. 1: Actual BS locations from a current cellular deployment. BSs are represented by large circles, and Voronoi cell boundaries are represented by thick lines. To minimize edge effects, the reference mobile is assumed to be located in the yellow zone in the center of the diagram.

II. NETWORK MODEL

A. Network Topology

In the network model, C BSs and M mobiles are confined to a finite area. As an example, Fig. 1 depicts an actual deployment of $C = 132$ BSs extracted from the OFCOM database for Vodafone in London¹. BSs are represented by large circles, and Voronoi cell boundaries are represented by thick lines. The network occupies 4 km^2 inside a square. The M mobiles within it are located according to a uniform clustering distribution with each mobile surrounded by an *exclusion zone* [13] with radius r_{ex} .

B. Propagation Model

At millimeter-wave frequencies, blockages by various obstacles often prevent LOS propagation, but reflections allow a non-line-of-sight (NLOS) propagation of multipath clusters to reach the receiver. Extensive measurement campaigns, such as those in [14], classify measurements

¹<http://www.sitefinder.ofcom.org.uk>

into LOS and NLOS categories, and find separate path-loss exponents and shadowing standard deviations for each category. Building upon these measurements, stochastic millimeter-wave propagation models (e.g., [10], [15]–[17]) characterize the blockages with a stochastic model, and then use random shape theory to determine the probability of LOS propagation. Such models show the strong dependence of the LOS probability upon the link length. In [15]–[17], a fairly accurate approximation is found by classifying all links shorter than a critical distance (the radius of an *LOS ball*) to be LOS, and all links longer to be NLOS. Such an approximation hardens the stochastic model into a deterministic one with a sharp transition at the critical distance. In this paper, we propose a refined deterministic model that allows for a more gradual transition from LOS to NLOS regions, thereby capturing the partial or occasional blocking that may occur at intermediate distances. The key to the model is the use of a nonlinear *tanh* function to capture the statistical dynamics of LOS and NLOS paths in a single function with a rapid, but not instantaneous, transition between predominately LOS and NLOS zones. The rate of the transition can be tuned to match the data for a given blockage model. For such a model, the blockage and LOS probabilities do not have to be assumed, links do not have to be identified as either LOS or NLOS, and both shadowing and fading can be seamlessly included. The fact that some short paths could have a higher attenuation than longer ones is taken into account by the shadowing, which induces a variability in the received power due primarily to partial blockages.

The propagation model comprises models for the area-mean power, the local-mean power, and the fading [18]. The area-mean power, which is the average received power in the network region, is a function of the distance d between a source and destination. The area-mean path-loss function is expressed as the attenuation power law

$$f(d) = \left(\frac{d}{d_0}\right)^{-\alpha(d)}, \quad d \geq d_0 \quad (1)$$

where $\alpha(d)$ is the attenuation power-law exponent, and d_0 is a reference distance that is less than or equal to r_{ex} . At microwave frequencies, the power-law exponent is approximately constant, but at millimeter-wave frequencies, its distance-dependence must be modeled.

Since the area-mean power is an average power over the network region, the distance-dependent model of the power-law exponent for millimeter-wave frequencies is an average over the LOS and NLOS network links. This model reflects the empirical fact that $\alpha(d)$ differs substantially for LOS and NLOS links, tending toward α_{min} for the usually shorter LOS links and tending

toward a much larger α_{max} for the usually longer NLOS links [14], [19], [20]. Empirical data, such as that shown in Fig. 2 of [14], indicates that there is a small range of link lengths for which there are significant numbers of both LOS and NLOS links within the network region. Therefore, $\alpha(d)$ is modeled as a monotonically increasing function:

$$\alpha(d) = \alpha_{min} + (\alpha_{max} - \alpha_{min}) \tanh(\mu d) \quad (2)$$

which indicates that $\alpha_{min} \leq \alpha(d) < \alpha_{max}$. The *transition parameter* μ , which can be determined by fitting to empirical data, controls the transition rate from α_{min} to a value close to α_{max} .

The local-mean received power at one end of a communication link is the product of the area-mean power and a factor due to large-scale terrain effects in the vicinity of the link. This factor is expressed as $10^{\xi/10}$, where ξ is the *shadowing factor* for the link. The shadowing factor can be derived from a deterministic terrain model or can be modeled as a random variable in a statistical model. In this paper, we assume lognormal shadowing in which the shadowing factors are independent, identically distributed, zero-mean Gaussian random variables with a distance-dependent variance.

For millimeter-wave frequencies, empirical data [14], [19], [20] indicates that the standard deviation of the shadowing factor differs substantially for LOS and NLOS links, tending toward σ_{min} for the usually shorter LOS links and tending toward a much larger σ_{max} for the usually longer NLOS links [14], [19], [20]. Since there is a small range of link lengths for which there are significant numbers of both LOS and NLOS links, the standard deviation of the shadowing factor for millimeter-wave frequencies is modeled as a monotonically increasing function:

$$\sigma_s(d) = \sigma_{min} + (\sigma_{max} - \sigma_{min}) \tanh(\mu d) \quad (3)$$

which indicates that $\sigma_{min} \leq \sigma_s(d) < \sigma_{max}$.

The fading is assumed to have a Nakagami distribution function. Since the received power for the longer NLOS links is due to multipath clusters, the fading becomes more severe. Therefore, in analogy with (1) and (2), a distance-dependent Nakagami parameter is modeled as a monotonically decreasing function:

$$m(d) = m_{max} - (m_{max} - m_{min}) \tanh(\mu d) \quad (4)$$

which indicates that $m_{min} \leq m(d) < m_{max}$. If $m(d)$ is constrained to be an integer, then we set it equal to the integer closest to the value of the right-hand side of (4).

This propagation model facilitates simple simulations of the performance of frequency-hopping millimeter-wave uplinks. The model has been validated for the outdoor urban propagation environment and some frequencies. Validation and the extraction of the model parameter values can be done for other propagation environments and frequencies as measurements become available. The propagation model could be replaced by or combined with more specific propagation models. Although the simulation complexity, and the time required for simulations might increase, the basic methodology described below would remain intact.

C. Beamforming

Because of the high propagation losses, high handover rates, intermittent connectivity, and power limitations of mobile transmitters at millimeter-wave frequencies, the antenna arrays at the BSs and mobiles will need to form highly directional beams for uplink transmissions [21]–[23]. The beams are fixed in space and each mobile aligns its antenna with one of beams of the base station. While spatial multiplexing is an option in 4G networks, the multiple-input multiple-output (MIMO) dimensions in 5G uplinks should be used for beamforming, which serves as a type of open-loop multiuser MIMO. Providing multiple layers to individual mobiles is impractical primarily because of the difficulty in obtaining and feeding back channel-state information when the handover rates are high, and the need for digital processing of multiple antenna outputs.

Densification, high mobility, and the severe impact of blockages at millimeter-wave frequencies cause frequent handovers and hence the need for rapid mutual beam alignments. Scanning over many angles and the contamination of the pilot signals carrying angle-of-arrival information are impediments to adaptive beams. *Sectorization*, which is the division of BS coverage into $\zeta > 1$ fixed angular sector beams centered at the BS, is used to reduce beam-alignment delays. Sectorization facilitates power control and the allocations of frequency-hopping patterns within each sector. Thus, we assume BS sectorization and adaptive beamforming for the mobiles. At millimeter-wave frequencies, the beams can be implemented using many antenna elements, perhaps hundreds, and hence they have narrow beamwidths and very small sidelobes and backlobes.

The scalar S_l , $l = 1, 2, \dots, \zeta C$, represents the l th sector or its receiver, and the scalar X_i , $i = 1, 2, \dots, M$, represents the i th mobile. The two-component column vector \mathbf{S}_l , $l = 1, 2, \dots, \zeta C$, represents the location of the l th sector receiver, and the two-component column vector \mathbf{X}_i ,

$i = 1, 2, \dots, M$, represents the location of the i th mobile.

Let \mathcal{X}_l denote the set of mobiles served by sector S_l . Let $X_r \in \mathcal{X}_j$ denote a reference mobile that transmits a desired signal to a reference receiver S_j . Let $\mathbf{g}(i)$ denote a function that returns the index of the sector serving X_i so that $X_i \in \mathcal{X}_l$ if $\mathbf{g}(i) = l$. The sector $S_{\mathbf{g}(i)}$ that serves mobile X_i is assumed to be the one with minimum local-mean path loss when the mainlobe of the transmit beam of X_i is aligned with the sector beam of $S_{\mathbf{g}(i)}$. Thus, the serving sector has index

$$\mathbf{g}(i) = \arg \max_l \{ 10^{\xi_{i,l}/10} f(\|\mathbf{S}_l - \mathbf{X}_i\|), X_i \in \mathcal{A}_l \} \quad (5)$$

where $\xi_{i,l}$ is a *shadowing factor* for the link from X_i to S_l , $f(\cdot)$ is the area-mean path-loss function, and \mathcal{A}_l denote the set of mobiles *covered* by the sector beam of S_l . The implication of (5) is that the mobile device will associate its uplink with the sector that receives the strongest signal from the device. While cell-range expansion in a HetNet might cause the downlink to follow a different association rule, this rule is reasonable for either a single-tier network or a HetNet with a decoupled uplink [6]. In the absence of shadowing, the serving sector will be the receiver that is closest to X_i . In the presence of shadowing, a mobile device may actually be associated with a sector that is more distant than the closest one if the shadowing conditions are sufficiently better.

Each sector-beam gain pattern is modeled by a two-level function with maximum constant gain over a mainlobe with beamwidth equal to $2\pi/\zeta$, and minimum constant gain over the sidelobes and backlobes. Let A_s denote the average gain of a sector beam. Then the *sector-beam gain pattern* associated with S_l may be expressed as

$$B_l(\theta) = \begin{cases} A_s[b + \zeta(1 - b)], & \psi_l \leq \theta \leq \psi_l + 2\pi/\zeta \\ A_s b, & \text{otherwise} \end{cases} \quad (6)$$

ψ_l is the offset angle of the beam pattern, and b is the relative sidelobe and backlobe level.

Each active mobile points its adaptive beam toward its associated BS. The antenna model, which is used to approximate the beamforming patterns, is illustrated in Fig. 2, while the values of beamwidth, mainlobe gain, and sidelobe gain are provided for both the mobile and base station in Table I. As in [15], the antenna pattern is modeled with two gains: one for the mainlobe with beamwidth Θ , and another for the sidelobes and backlobes. Let A_m denote the average gain of an adaptive mobile beam. Then the *mobile-beam gain pattern* in the direction of the reference

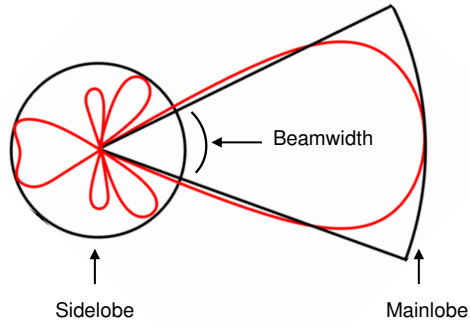


Fig. 2: Antenna model (See also Fig1.b of [15]).

	Mobile	BS sector
Beamwidth	Θ	$\frac{2\pi}{\zeta}$
Mainlobe gain	$A_m[a + \frac{2\pi(1-a)}{\Theta}]$	$A_s[b + \zeta(1-b)]$
Sidelobe gain	$A_m a$	$A_s b$

TABLE I: Summary of the antenna characteristics.

receiver S_j due to the angular offset of this beam pattern may be expressed as

$$b_{i,j} = \begin{cases} A_m[a + \frac{2\pi(1-a)}{\Theta}], & \frac{(\mathbf{S}_j - \mathbf{X}_i)^T (\mathbf{S}_{g(i)} - \mathbf{X}_i)}{\|\mathbf{S}_j - \mathbf{X}_i\| \|\mathbf{S}_{g(i)} - \mathbf{X}_i\|} > \cos\left(\frac{\Theta}{2}\right) \\ A_m a, & \text{otherwise} \end{cases} \quad (7)$$

where $\|\cdot\|$ is the Euclidean norms, the superscript T denotes the transpose, and a is the relative sidelobe and backlobe level. The main idea behind (7) is to set the mobile's antenna gain to its mainlobe level when it is facing the reference base station and to set it to its sidelobe level when it is facing away.

D. Frequency Hopping and Intersector Interference

Frequency hopping [18] may be used in SC-FDMA uplink systems to provide the diversity that will mitigate the effects of frequency-selective fading and intersector interference. Because of network synchronization and similar propagation delays for the mobiles associated with a cell

sector, synchronous orthogonal frequency-hopping patterns can be allocated so that at any given instant in time, there is no *intrasector* interference. The frequency-hopping patterns transmitted by mobiles in other sectors are not generally orthogonal to the patterns in a reference sector, and hence produce *intersector* interference. The varying propagation delays from the interfering mobiles cause their frequency-hopping signals to be asynchronous with respect to the desired signal. Duplexing prevents uplink interference from downlink transmissions.

Each mobile uses a frequency-hopping pattern over a hopset with L disjoint frequency channels. Let L_l , $l = 1, 2, \dots, \zeta C$, denote positive integer divisors of L such that $L/L_l \geq 2$. Each mobile in \mathcal{X}_l is assigned a distinct block of L_l contiguous frequency channels during each of its hop intervals, and the block may change to any of L/L_l disjoint spectral regions with every hop. Consider an uplink *reference signal* that traverses a reference link from a reference mobile X_r to a reference receiver S_j . To minimize edge effects, the reference mobile is assumed to be located in the yellow zone in the center of Fig. 1. Because of a possible incomplete spectral overlap, the received interference power from mobile X_i at S_j when the mobile's signal collides with the reference signal is reduced by the *spectral factor*

$$F_l = \min(L_j/L_l, 1). \quad (8)$$

Associated with each potentially interfering mobile, which is assumed to transmit throughout a subframe or not at all, is a hop transition time $t_{i,j}$ at S_j relative to the hop transition time of a pair of hop intervals of the reference signal. Fig. 3 illustrates the relative timing of the signals from the reference mobile X_r and the interfering mobile X_i . We assume a static topology, no handoffs, continual transmissions, and fixed frequency assignments throughout the duration of the subframe. The reference mobile transmits a turbo codeword of duration $2T$, which is aligned with the subframe. It is assumed that the frequency separation of the two frequency channels of the two slots is sufficient for independent fading of fixed amplitude in each slot. If the sector receivers and mobiles are synchronized, then

$$t_{i,j} = [(\|\mathbf{S}_j - \mathbf{X}_r\| - \|\mathbf{S}_j - \mathbf{X}_i\|)/c] \bmod T \quad (9)$$

where c is the speed of an electromagnetic wave. As illustrated in Fig. 3, the reference signal encounters four time periods of potential interference from an active mobile X_i : $0 \leq t \leq t_{i,j}$, $t_{i,j} \leq t \leq T$, $T \leq t \leq t_{i,j} + T$, and $t_{i,j} + T \leq t \leq 2T$. The generic index $k \in \{1, 2, 3, 4\}$, denotes

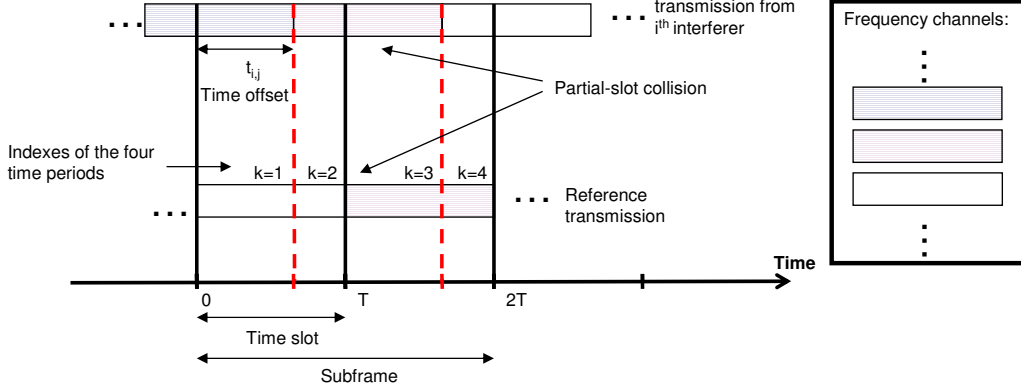


Fig. 3: Illustration of co-channel interference at sector receiver S_j produced by an interfering mobile X_i and arriving with a relative timing offset of $t_{i,j}$. Each block in the illustration represents a hop, and the selected channel is indicated by the shading of the block. A partial-slot collision is indicated, where the interfering mobile has selected the frequency channel used by the reference mobile during the second slot of the subframe. However, due to the asynchronism, the collision only extends for part of the slot.

a time period of the subframe with duration that varies with each $t_{i,j}$. In the example provided in Fig. 3, co-channel interference occurs during the third time period, where the interfering mobile has selected the frequency channels used by the reference mobile. The *fractional duration* of each of the four subframe time periods relative to the subframe period $2T$ are

$$C_{i,j,k} = \begin{cases} \frac{t_{i,j}}{2T}, & k = 1, 3 \\ \frac{T-t_{i,j}}{2T}, & k = 2, 4 \end{cases}. \quad (10)$$

The set of indices of potentially interfering mobiles is $\mathcal{S} = \{i : X_i \notin \mathcal{X}_j\}$. Let N_l denote the number of mobiles associated with sector S_l . Because of the required orthogonality of frequency blocks assigned to mobiles within each sector, $N_l \leq L/L_l$ and any additional mobiles within the sector are reassigned to other sectors. Each additional mobile is served by the sector from which it receives the next highest power. If all the sectors happened to have excess mobiles, then some mobiles would be denied service. In view of the potential spectral overlaps, the maximum number of interfering mobiles within a sector during a subframe time period is $\min[\max(L_j/L_l, 1), N_l]$. Let $\mathcal{S}_k \subset \mathcal{S}$ denote the set of interfering mobiles during subframe time period k . If $N_l \leq \max(L_j/L_l, 1)$, then all N_l mobiles in sector l are in \mathcal{S}_k . If $N_l > \max(L_j/L_l, 1)$, then some

of the mobiles in sector l cannot cause interference during subframe time period k . In that case, we approximate by randomly selecting a subset of the N_l mobiles to be included in \mathcal{S}_k .

Let $q_{i,k}$ denote the probability that the signal from a potentially interfering mobile collides with the reference signal during subframe time period k , $1 \leq k \leq 4$. The *activity probability* p_i is the probability that mobile X_i transmits throughout the time interval $[0, 2T)$. Assuming uniformly distributed frequency-hopping patterns that are orthogonal within each sector,

$$q_{i,k} = \frac{\max(N_{g(i)}L_{g(i)}, L_j)}{L}p_i, \quad i \in \mathcal{S}_k, \quad 1 \leq k \leq 4 \quad (11)$$

and $q_{i,k} = 0$, otherwise.

E. SINR

The instantaneous signal-to-interference-and-noise ratio (SINR) at sector receiver S_j when the desired signal is from $X_r \in \mathcal{X}_j$ fluctuates because potentially interfering signals do not always coincide with the reference signal in time or frequency. Pilot sequences are used to estimate the complex fading amplitudes in the receiver. Therefore, the performance of the reference receiver is primarily a function of the *average SINR* defined as the ratio of the average power of the signal to the average power of the noise and interference, where the average is over the time interval of a subframe and turbo codeword. It is assumed that the adaptive beam of reference mobile X_r is perfectly aligned with the sector beam. The average SINR during a subframe is

$$\gamma_{r,j} = \frac{\bar{\rho}_{r,j}}{\mathcal{N} + \sum_{k=1}^4 \sum_{i \in \mathcal{S}_k} I_{i,k} \rho_{i,j,k} C_{i,j,k}} \quad (12)$$

where \mathcal{N} is the noise power, $\bar{\rho}_{r,j}$ is the average received power from reference mobile X_r , and $\rho_{i,j,k}$ is the received power from an interference signal that collides with the reference signal during subframe time period k . The indicators $I_{i,k}$ are Bernoulli random variables with probabilities

$$P[I_{i,k} = 1] = q_{i,k}, \quad P[I_{i,k} = 0] = 1 - q_{i,k} \\ i \in \mathcal{S}_k, \quad 1 \leq k \leq 4. \quad (13)$$

Let $g_{r,j,1}$ and $g_{r,j,2}$ denote the unit-mean power gains due to the independent fading of the frequency-hopping reference signal in subframe slots 1 and 2, respectively. The power gain of

independent Nakagami fading with parameter $m_0 = m_{r,j}$ in each slot has the gamma density function:

$$h_{r,j}(x) = \frac{m_0^{m_0} x^{m_0-1} \exp(-m_0 x)}{\Gamma(m_0)} u(x) \quad (14)$$

where $u(x) = 1$, $x \geq 0$, and $u(x) = 0$, otherwise. The average power gain due to fading is $\bar{g}_{r,j} = (g_{r,j,1} + g_{r,j,2})/2$. Using (14), we obtain the density function of $\bar{g}_{r,j}$:

$$h_0(x) = \frac{(2m_0)^{2m_0} x^{2m_0-1} \exp(-2m_0 x)}{\Gamma(2m_0)} u(x) \quad (15)$$

which is the power of a Nakagami random variable with parameter $2m_0$. This doubling of the Nakagami parameter indicates the beneficial effect of the frequency hopping in mitigating frequency-selective fading. Let P_r denote the power from X_r that would be received at the reference distance d_0 with maximum antenna-pair gain in the absence of shadowing and fading. The average received power from reference mobile X_r is

$$\bar{\rho}_{r,j} = P_r \bar{g}_{r,j} 10^{\xi_{r,j}/10} f(d_r) \quad (16)$$

where $d_r = \|\mathbf{S}_j - \mathbf{X}_r\|$ is the length of the reference link.

Let $g_{i,j,k}$ denote the fading gain of the signal from mobile X_i at S_j during time interval k . Assuming that the bandwidths of the L/L_l and L/L_j disjoint spectral regions exceed the coherence bandwidth, the $\{g_{i,j,k}\}$ are independent for each hop interval with unit-mean, and $g_{i,j,k} = a_{i,j,k}^2$, where $a_{i,j,k}$ has a Nakagami distribution with distance-dependent parameter $m_{i,j}$. Let P_i denote the power from X_i that would be received at the reference distance d_0 with maximum antenna-pair gain in the absence of shadowing and fading. Allowing for the spectral and beam factors, the received power from X_i at S_j , $i \in \mathcal{S}_k$, during time interval k is

$$\rho_{i,j,k} = P_i g_{i,j,k} 10^{\xi_{i,j}/10} f(\|\mathbf{S}_j - \mathbf{X}_i\|) F_{g(i)} \frac{b_{i,j} B_j(\theta_{i,j})}{B_{\max}} \quad (17)$$

$$i \in \mathcal{S}_k, \quad 1 \leq k \leq 4$$

where the *maximum antenna-pair gain* is

$$B_{\max} = A_s A_m [b + \zeta(1-b)] \left[a + \frac{2\pi(1-a)}{\Theta} \right] \quad (18)$$

and $\theta_{i,j}$ is the arrival angle at S_j of a signal from X_i .

F. Power Control

The synchronous, orthogonal uplink signals in a sector ensure the absence of near-far problems and intrasector interference in principle. However, power control is needed to limit the potential intrasector interference caused by synchronization errors and hardware imperfections. Closed loop uplink power control may be implemented by monitoring the received powers of the SC-FDMA signals at the sector receiver, and then feeding back control commands to the sector mobiles that constrain the local-mean power received from each sector mobile, which is assumed to have its beam aligned with its associated sector beam. To provide mobiles with some flexibility in exploiting favorable channel conditions, *fractional power control* of the constrained local-mean power implies that

$$P_r [10^{\xi_{r,j}/10} f(d_r)]^\delta = P_i [10^{\xi_{i,g(i)}/10} f(\|\mathbf{S}_{g(i)} - \mathbf{X}_i\|)]^\delta, \\ i \in \mathcal{S}_k, 0 < \delta < 1 \quad (19)$$

where δ is the *power-control parameter*. If $\delta = 0$, there is no power control, and transmitter powers are all equal. If $\delta = 1$, full power control forces the received local-mean powers from all mobiles to be equal. If $0 < \delta < 1$, then decreasing δ improves the performance of some mobiles in a sector while increasing the interference in neighboring sectors.

Substituting (16), (17), and (19) into (12), we obtain

$$\gamma_{r,j} = \frac{\bar{g}_{r,j}}{\Gamma_0^{-1} + \sum_{k=1}^4 \sum_{i \in \mathcal{S}_k} I_{i,k} \Omega_{i,j} g_{i,j,k} C_{i,j,k}} \quad (20)$$

where

$$\Omega_{i,j} = \frac{10^{[\xi_{i,j} - \delta \xi_{i,g(i)} + (\delta-1)\xi_{r,j}]/10} f(\|\mathbf{S}_j - \mathbf{X}_i\|) F_{g(i)} b_{i,j} B_j(\theta_{i,j})}{[f(d_r)]^{1-\delta} [f(\|\mathbf{S}_{g(i)} - \mathbf{X}_i\|)]^\delta B_{\max}} \quad (21)$$

is the ratio of the interference power from X_i to the reference-signal power, and

$$\Gamma_0 = \frac{P_r}{\mathcal{N}} 10^{\xi_{r,j}/10} f(d_r) \quad (22)$$

is the signal-to-noise ratio (SNR) at the sector receiver in the absence of fading. Because of the division in (21), $\Omega_{i,j}$ does not depend on the average gains A_s and A_m . The *reference SNR* is P_r/\mathcal{N} , which is the received SNR at distance d_0 when the maximum antenna-pair gain occurs and shadowing and fading are absent.

III. OUTAGE PROBABILITY

Let β denote the minimum average SINR required for reliable reception of a signal from X_r at its serving sector receiver S_j , $j = \mathbf{g}(r)$. An *outage* occurs when the average SINR of a signal from X_r falls below β . The value of β sets a limit on the code-rate R of the uplink, which is expressed in units of bits per channel use (bpcu), and depends on the modulation and coding schemes, and the overhead losses due to pilots, cyclic prefixes, and equalization methods. The exact dependence of R on β can be determined empirically through tests or simulation.

The set of $\{\Omega_{i,j}\}$, $i \in \mathcal{S}_k$, for reference receiver S_j is represented by the vector Ω_j . Conditioning on Ω_j , the *outage probability* of a desired signal from $X_r \in \mathcal{X}_j$ that arrives at S_j is

$$\epsilon = P[\gamma_{r,j} \leq \beta | \Omega_j]. \quad (23)$$

Because it is conditioned on Ω_j , the outage probability depends on the particular network realization, which has dynamics over timescales that are much slower than the fading or frequency hopping. We define

$$\beta_0 = 2\beta m_0, \quad z = \Gamma_0^{-1} \quad (24)$$

where the Nakagami parameter $m_0 = [m_{r,j}]$ for the reference uplink signal is assumed to be a positive integer. A derivation similar to the one in [8] yields

$$\epsilon = 1 - e^{-\beta_0 z} \sum_{s=0}^{2m_0-1} (\beta_0 z)^s \sum_{t=0}^s \frac{z^{-t}}{(s-t)!} H_t(\Omega) \quad (25)$$

where

$$H_t(\Omega) = \sum_{\substack{\ell_{ik} \geq 0 \\ \sum_{k=1}^4 \sum_{i \in \mathcal{S}_k} \ell_{ik} = t}} \prod_{k=1}^4 \prod_{i \in \mathcal{S}_k} G_{\ell_{ik}}(i, j, k) \quad (26)$$

the summations in (26) are over all sets of nonnegative indices that sum to t ,

$$G_\ell(i, j, k) = \begin{cases} 1 - q_{i,k}(1 - \Psi_{i,j,k}^{m_{i,j}}), & \ell = 0 \\ \frac{q_{i,k} \Gamma(\ell + m_{i,j})}{\ell! \Gamma(m_{i,j})} \left(\frac{\Omega_{i,j} C_{i,j,k}}{m_{i,j}} \right)^\ell \Psi_{i,j,k}^{m_{i,j} + \ell} & \ell > 0 \end{cases} \quad (27)$$

and

$$\Psi_{i,j,k} = \left(\beta_0 \frac{\Omega_{i,j} C_{i,j,k}}{m_{i,j}} + 1 \right)^{-1}, \quad i \in \mathcal{S}_k, \quad 1 \leq k \leq 4. \quad (28)$$

IV. NUMERICAL RESULTS

In the following examples, statistical performance metrics are calculated by using a Monte Carlo approach with N simulation trials. In each simulation trial, a realization of the network of Fig. 1 is obtained by placing M mobiles within it according to a uniform clustering distribution with $r_{ex} = d_0 = 0.004$ km. Randomly generated shadowing factors are used in the association of mobiles with cell sectors and in other computations. Independent shadowing is assumed among all uplinks, an assumption that becomes increasingly accurate as densification limits the number of mobiles with beams pointing toward a sector beam.

The code rate permitted by the threshold is given by

$$R = \log_2(1 + l_s \beta) \quad (29)$$

where $l_s = 0.794$ corresponds to a 1 dB loss relative to the Shannon bound for complex discrete-time AWGN channels. The density of mobiles in a network of area A_{net} is $\lambda = M/A_{\text{net}}$. The outage probability ϵ_i of the reference link for simulation trial i is computed by applying (25)–(28). The *throughput* of the reference uplink for simulation trial i is $R(1 - \epsilon_i)$. The average outage probability over all the simulation trials is

$$\bar{\epsilon} = \frac{1}{N} \sum_{i=1}^N \epsilon_i. \quad (30)$$

The maximum rate of successful data transmissions per unit area is characterized by the *area spectral efficiency*, defined as

$$\mathcal{A} = \lambda R (1 - \bar{\epsilon}) \quad (31)$$

where the units are bits per channel use per unit area.

To avoid edge effects, the performance is measured for a reference mobile placed in the yellow shaded area of Fig. 1, which is a 1 km by 1 km square located in the middle of the network. To consider the effect of BS densification, the relative topology of the BSs and the density of mobiles served within each subframe $\lambda = 100/km^2$ are maintained while the size of the network is scaled (dimensions redefined). For a fixed number of BSs, each scaling changes the number of mobiles per sector and the transmission distances. In considering the effects of intersector interference, only the strongest 30 signals were used, as the attenuation of further signals was severe enough to make their individual effects negligible.

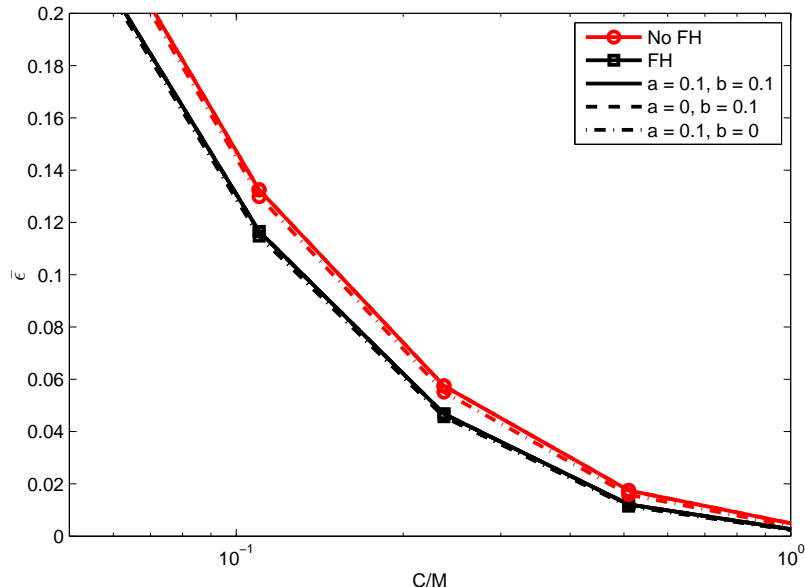


Fig. 4: Average outage probability as a function of densification for both frequency hopping and its absence. Densification is quantified by the average number of base stations per mobile. In this example, a user density of $\lambda = 100$ mobiles per km^2 is assumed.

The ratio C/M serves as a measure of the densification of the BSs. To capture the impact of densification, we take into account the decrease in the *typical link-length* d_r of the reference link and the consequent increase in Γ_0 as C/M increases. The typical link-length is defined as one-fourth of the average separation between BSs. For a fixed density of mobiles, the average area associated with a cell is inversely proportional to C/M , and hence the average cell radius and a *typical* d_r are proportional to $1/\sqrt{C/M}$. For the range of C/M of interest, we consider

$$d_r = \frac{d_{r0}}{\sqrt{C/M}}, \quad 0.05 \leq C/M \leq 1 \quad (32)$$

where $d_{r0} = 25$ m is the typical link length when $C/M = 1$.

Unless otherwise stated the reference SNR in the examples is $P_r/\mathcal{N} = 70$ dB. This SNR might be realized as follows. The transmitter output power is 30 dBm, the path loss at the reference distance is 90 dB, the maximum antenna-pair gain is 40 dB, and thus $P_r = -20$ dBm. The noise power spectral density is -174 dBm/Hz, the reference-signal bandwidth is 1 GHz, the noise figure is 6 dB, and thus $\mathcal{N} = -90$ dBm.

The slot duration is $T = 0.5$ ms, and the common activity factor is $p_i = 1$. Unless otherwise stated, frequency hopping is used, and other parameter values are $L/L_j = L/L_l = 10$, $\mu =$

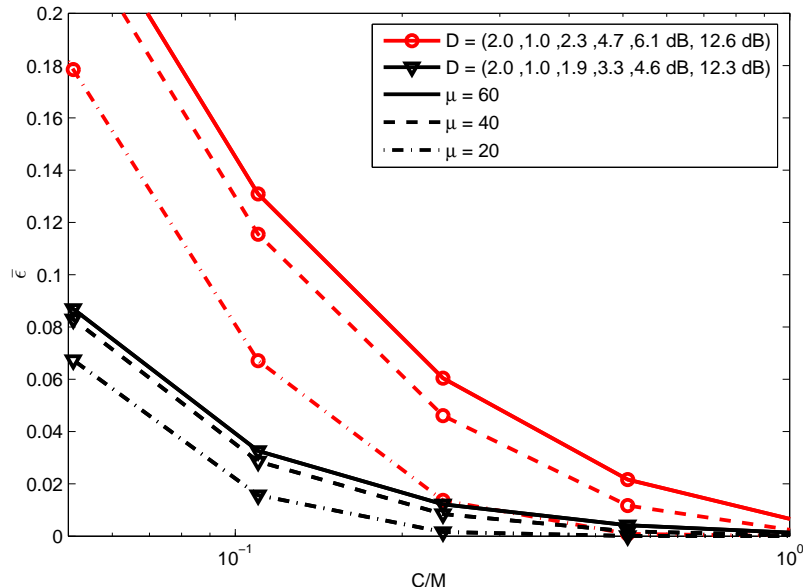


Fig. 5: Average outage probability for several values of the transition parameter μ and two sets of propagation parameters.

$20/km$, $b = 0.01$, $\zeta = 24$, $\Theta = 0.1\pi$ radians, $a = 0.1$, $\beta = 3$ dB, $\delta = 0.1$, and $N = 10^5$. Unless otherwise stated, the propagation parameters are $D = (m_{\max}, m_{\min}, \alpha_{\min}, \alpha_{\max}, \sigma_{\min}, \sigma_{\max}) = (2.0, 1.0, 2.3, 4.7, 6.1, 12.6)$ dB, which are similar to those expected in a harsh urban environment such as central New York when transmitting in the vicinity of 73 GHz [14].

Figures 4-7 depict the average outage probability $\bar{\epsilon}$ for a typical link as a function of the densification and various parameter values. The primary reasons for the monotonic decrease in $\bar{\epsilon}$ with densification are the increases in Γ_0 and the reduced path loss and shadowing experienced by the reference signal. Fig. 4 illustrates the significant benefit of frequency hopping. In the absence of frequency hopping, the reference signal is assumed to experience constant fading over a subframe, which is valid if subframe duration is less than the coherence time. The figure shows that the relative decrease in $\bar{\epsilon}$ due to the use of frequency hopping increases with densification. A viable network would require an $\bar{\epsilon}$ below 0.05, which in this example requires $C/M \gtrsim 0.2$ if frequency hopping is used and $C/M \gtrsim 0.35$ if it is not. The curves for $a = 0.1$, $b = 0$ and $a = 0$, $b = 0.1$ indicate that decreasing either the sector-beam sidelobe level below $b = 0.1$ or the mobile-beam sidelobe level below $a = 0.1$ has a very small effect on $\bar{\epsilon}$.

Fig. 5 compares the effects of several values of the transition parameter μ and two sets of

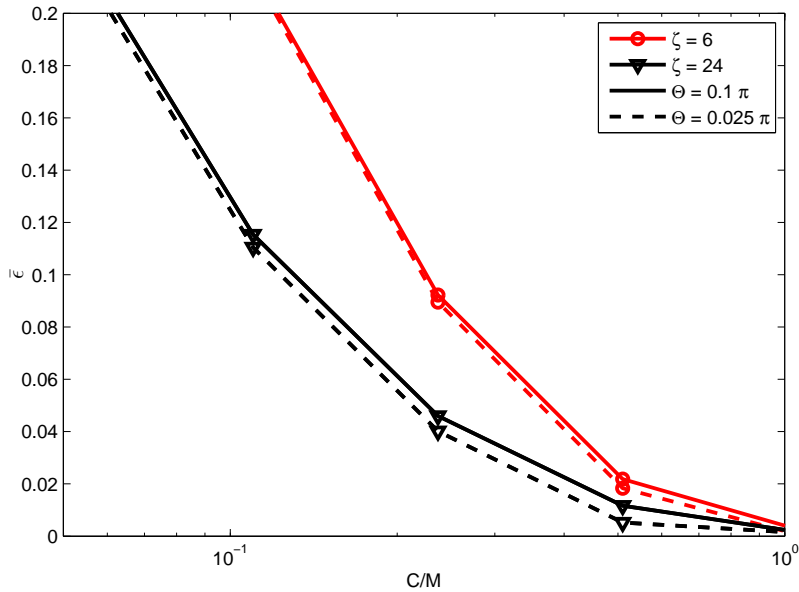


Fig. 6: Average outage probability for several values of the mobile-beam beamwidth Θ and the number of sectors ζ .

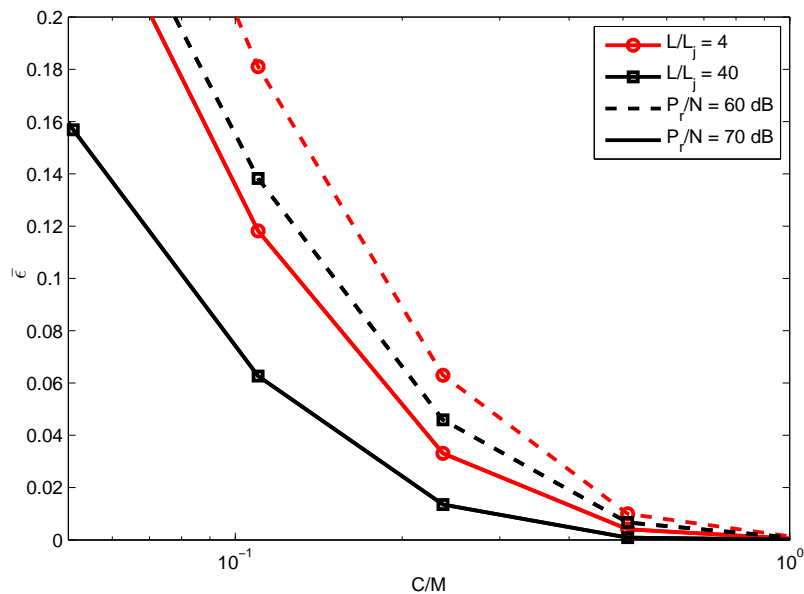


Fig. 7: Average outage probability for several values of L/L_j and P_r/N .

propagation parameters. The set $D = (2.0, 1.0, 2.3, 4.7, 6.1 \text{ dB}, 12.6 \text{ dB})$ is based on data for New York, whereas the set $D = (2.0, 1.0, 1.9, 3.3, 4.6 \text{ dB}, 12.3 \text{ dB})$ is based on data for Austin, Texas [14]. The figure illustrates the benefits of low transition rates and less congested urban networks. The six curves in the figure converge toward each other as the densification increases

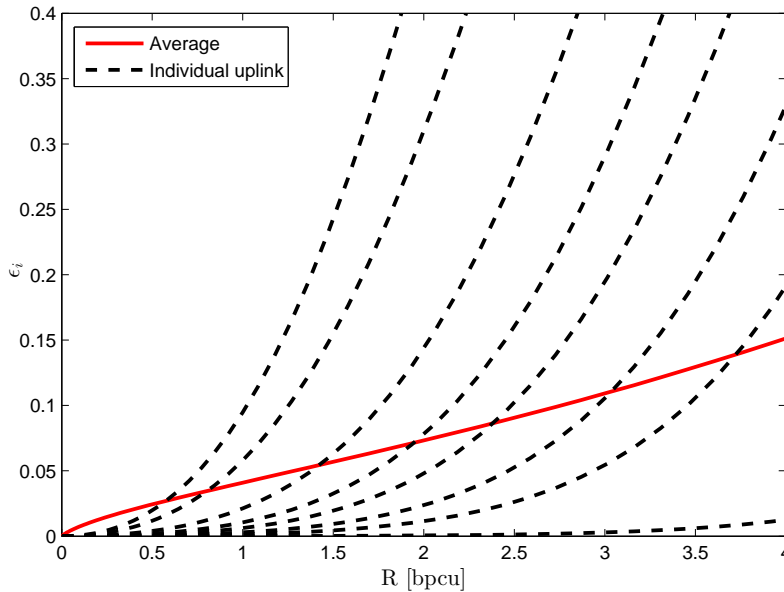


Fig. 8: Outage probabilities of eight uplinks and the average outage probability over all the uplinks as functions of the code rate for $C/M = 0.1$ and a single simulation trial.

because then the typical link lies in the LOS region with similar parameter values for both New York and Austin.

Fig. 6 compares the effects of several values of the mobile beamwidth Θ and the number of sectors ζ . A decrease in Θ is of minor importance, whereas an increase in ζ is much more important, particularly for high levels of densification. In this figure, $P_r/\mathcal{N} = 70$ dB is maintained for all curves. However, if instead the average gains of the antennas are maintained, then the maximum antenna-pair gain increases with the increase in the number of sectors because of their narrower beamwidths. As a result, P_r/\mathcal{N} increases, and there is a further decrease in the average outage probability.

Fig. 7 compares the effects of several values of L/L_j and P_r/\mathcal{N} . For a fixed P_r/\mathcal{N} , a decrease in L/L_j corresponds to a decrease in the total available bandwidth relative to the reference-signal bandwidth. The figure shows that decreasing L/L_j by an order of magnitude causes a substantial increase in $\bar{\epsilon}$ due to the decreased effectiveness of the frequency hopping in enabling the reference signal to avoid interference. However, the increase in $\bar{\epsilon}$ is less significant as the densification increases, which indicates the diminishing importance of the intercell interference. A further indication of the predominance of the noise in limiting performance is the substantial

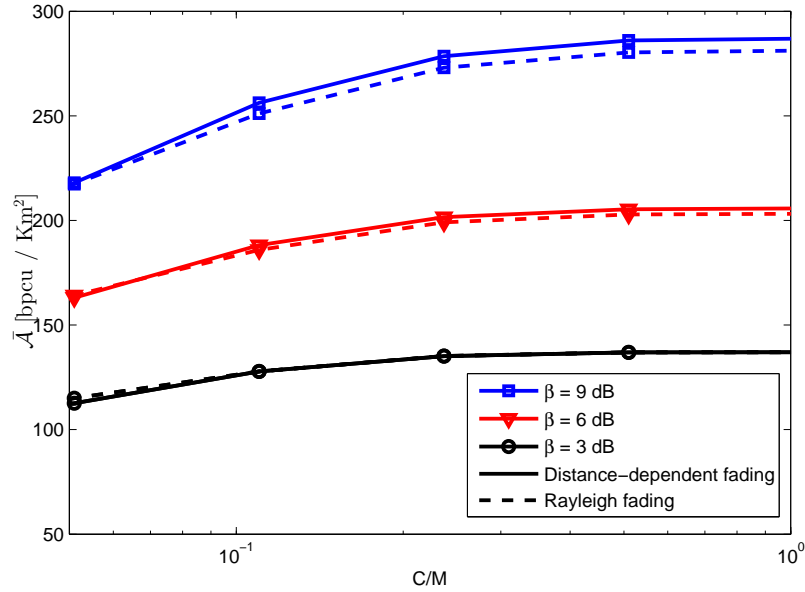


Fig. 9: Area spectral efficiency for three values of the SINR threshold and both distance-dependent and Rayleigh fading

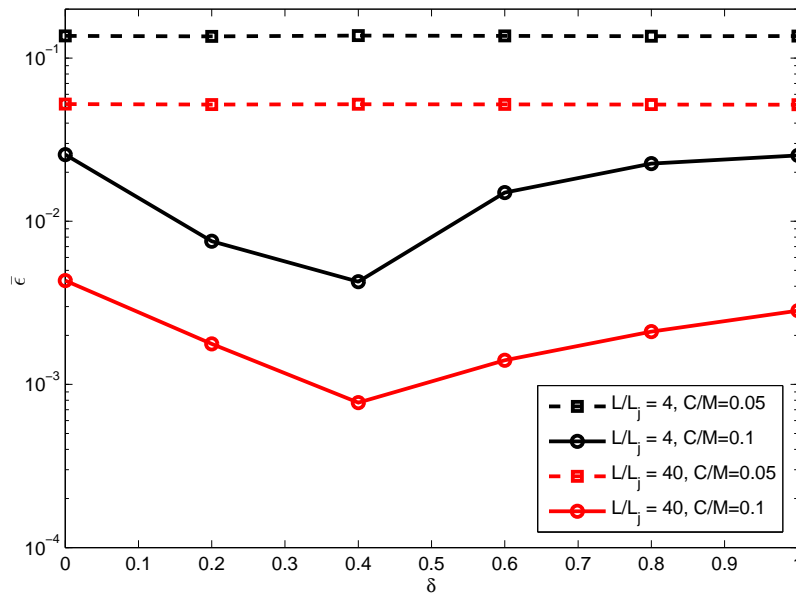


Fig. 10: Average outage probability as a function of the power-control parameter.

increase in $\bar{\epsilon}$ when $\bar{\epsilon} > 0.02$ and P_r/\mathcal{N} is reduced by 10 dB. Since beamforming and sufficient densification provide a noise-limited performance, there is little or no need for uplink scheduling to eliminate pilot contamination or interference among mobiles.

In Fig. 8, outage probabilities are plotted as functions of the code rate R for $C/M = 0.1$ and a single simulation trial. The dashed lines in the figure were generated by selecting eight random uplinks in the network and computing each outage probability. The average over all the uplinks is represented by the solid line. Despite the use of fractional power control, there is considerable variability in the dependence of the outage probability on the code rate due to the irregular network topology, which results in cell sectors of variable areas and numbers of mobiles.

Increases in the SINR threshold β of the network links increase the outage probability. However, for sufficiently large values of C/M and hence Γ_0 , this effect is minor compared with increased code rate that can be accommodated. As a result, the area spectral efficiency \mathcal{A} increases significantly, as illustrated in Fig. 9. Although high code rates lead to high values of area spectral efficiency, they also lead to high outage probabilities for many network links, as illustrated in Fig. 8. Therefore, a compromise solution in choosing the code rate will be necessary. Fig. 9 also illustrates that mild distance-dependent fading modeled in this paper provides an insignificant improvement relative to Rayleigh fading.

Figure 10 illustrates the effect of fractional power control on the average outage probability. The choice of the power-control parameter is largely irrelevant if $C/M < 0.1$. If $C/M \geq 0.1$ the optimal value of the power-control parameter is $\delta \approx 0.4$, but the outage probability is low for all choices of δ .

V. CONCLUSIONS

This paper derives an analytical model for calculating the outage probability and area spectral efficiency for frequency-hopping millimeter-wave uplinks that are strong candidates for use in 5G networks. The model includes the effects of millimeter-wave propagation, directional beams, frequency hopping, an arbitrary network topology, and the assignment of frequency blocks to mobiles. This paper applies deterministic geometry, which enables the accommodation of actual base-station topologies, rather than stochastic geometry, which usually relies on Poisson-distributed ones. In contrast to other propagation models, the propagation model in this paper is based on the direct application of received-power data. Numerical examples illustrate the effects of various features and parameters. The BS densification is shown to have critical importance in achieving good network performance. The significance of the intercell interference is greatly

reduced because of the highly directional sectorization and beamforming. The usefulness of frequency hopping in compensating for frequency-selective fading and reducing interference is illustrated. The benefits of increased sectorization, low transition rates, increased available bandwidth, and less congested urban networks are illustrated. For a sufficient degree of densification, the area spectral efficiency increases with the code rate despite the increase in the outage probability. However, a high code rate leads to high outage probabilities for many network links, and a compromise solution in choosing the code rate will be necessary. The minor importance of the power-control parameter of the fractional power control is shown. While the numerical results in this paper correspond to a representative example network, the methodology is general enough to be extended to a wide class of future-generation wireless networks.

REFERENCES

- [1] J. G. Andrews, S. Buzzi, W. Choi, S. V. Hanly, A. Lozano, A. C. K. Soong, and J. C. Zhang, "What will 5G be?," *IEEE J. Sel. Areas Commun.*, vol. 32, no. 6, pp. 1065-1082, June 2014.
- [2] P. Wang, Y. Li, L. Song, and B. Vucetic, "Multi-gigabit millimeter wave wireless communications for 5G: From fixed access to cellular networks," *IEEE Commun. Mag.*, vol. 53, no. 1, pp. 168-178, Jan. 2015.
- [3] S. Deb and P. Monogioudis, "Learning-based uplink interference management in 4G LTE cellular systems," *IEEE/ACM Trans. Networking*, vol. 23, pp. 398-411, April 2015.
- [4] N. Abu-Ali, A.-E. M. Taha, M. Salah, and H. Hassanein, "Uplink scheduling in LTE and LTE-Advanced: Tutorial, survey and evaluation Framework," *IEEE Commun. Surveys Tuts.*, vol. 16, pp. 1239-1265, third quarter 2014.
- [5] G. Ku and J. M. Walsh, "Resource allocation and link adaptation in LTE and LTE Advanced: A Tutorial," *IEEE Commun. Surveys Tuts.*, vol. 17, pp. 1605-1633, third quarter 2015.
- [6] F. Boccardi, J. G. Andrews, H. Elshaer, M. Dohler, S. Parkvall, P. Popovski, and S. Singh, "Why to decouple the uplink and downlink in cellular networks and how to do it," *IEEE Commun. Mag.*, vol. 54, no. 3, pp. 110-117, Mar. 2016.
- [7] D. Torrieri, S. Talarico, and M. C. Valenti, "Performance analysis of fifth-generation cellular uplink," in *Proc. IEEE Military Communications Conference (MILCOM)*, (Tampa, FL), Oct. 2015.
- [8] D. Torrieri and M. C. Valenti, "The outage probability of a finite ad hoc network in Nakagami fading," *IEEE Trans. Commun.*, vol. 60, no. 11, pp. 3509-3518, Nov. 2012.
- [9] M. Haenggi, *Stochastic Geometry for Wireless Networks*, Cambridge University Press, 2013.
- [10] M. Di Renzo, "Stochastic geometry modeling and analysis of multi-tier millimeter wave cellular networks," *IEEE Trans. Wireless Commun.*, vol. 14, no. 9, pp. 5038-5057, Sept. 2015.
- [11] M.C. Valenti, D. Torrieri, and S. Talarico, "A direct approach to computing spatially averaged outage probability," *IEEE Commun. Letters*, vol. 18, no. 7, pp. 1103-1106, July 2014.
- [12] Y. Li, F. Baccelli, H. S. Dhillon, and J. G. Andrews, "Statistical modeling and probabilistic analysis of cellular networks with determinantal point processes," *IEEE Trans. Commun.*, vol. 63, no. 9, pp. 3405-3422, Sept. 2015.
- [13] D. Torrieri and M. C. Valenti, "Exclusion and guard zones in DS-CDMA ad hoc networks," *IEEE Trans. Commun.*, vol. 61, no. 6, pp. 2468-2476, June 2013.

- [14] T. S. Rappaport, G. R. MacCartney, M.K. Samimi, and S. Sun, "Wideband Millimeter-wave propagation measurements and channel models for future wireless communication system design," *IEEE Trans. Commun.*, vol. 63, no. 9, pp. 3029-3056, Sept. 2015.
- [15] T. Bai, and R. W. Heath Jr., "Coverage and rate analysis for millimeter wave cellular networks," *IEEE Trans. Wireless Commun.*, vol. 14, no. 2, pp. 1100-1114, Feb. 2015.
- [16] S. Talarico and M. C. Valenti, "Frequency hopping on a 5G millimeter-wave uplink," in *Proc. Asilomar Conf. on Signals, Sys., & Comp.*, (Pacific Grove, CA), Nov. 2015.
- [17] K. Venugopal, M.C. Valenti, and R. W. Heath Jr., "Device-to-device millimeter wave communications: Interference, coverage, rate, and finite topologies," *IEEE Trans. Wireless Commun.*, to appear.
- [18] D. Torrieri, *Principles of Spread-Spectrum Communication Systems, 3rd ed.*, Springer, 2015.
- [19] S. Rangan, T. S. Rappaport, and E. Erkip, "Millimeter-wave cellular wireless networks: Potentials and challenges," *Proc. IEEE*, vol. 102, no. 3, pp. 366-385, Mar. 2014.
- [20] M. R. Akdeniz, Y. Liu, M. K. Samimi, S. Sun, S. Rangan, T. S. Rappaport, and E. Erkip, "Millimeter wave channel modeling and cellular capacity evaluation," *IEEE J. Selected Areas Commun.*, vol. 32, no. 6, pp. 1164-1179, June 2014.
- [21] H. Shokri-Ghadikolaei, C. Fischione, G. Fodor, P. Popovski, and M. Zorzi, "Millimeter wave cellular networks: A MAC layer perspective," *IEEE Trans. Commun.*, vol. 63, no. 10, pp. 3437-3458, Oct. 2015.
- [22] K. Zheng, L. Zhao, J. Mei, B. Shao, W. Xiang, and L. Hanzo, "Survey of large-scale MIMO systems," *IEEE Commun. Surveys Tuts.*, vol. 17, pp. 1738-1760, third quarter 2015.
- [23] S. Sun, T. S. Rappaport, R. W. Heath Jr., A. Nix, and S. Rangan, "MIMO for millimeter-wave wireless communications: Beamforming, spatial multiplexing, or both?," *IEEE Commun. Mag.*, vol. 52, no. 12, pp. 110-121, Dec. 2014.